

Nodal topology in d -wave superconducting monolayer FeSe

Takeru Nakayama^{1,*}, Tatsuya Shishidou², and Daniel F. Agterberg²

¹*The Institute for Solid State Physics, The University of Tokyo,
5-1-5 Kashiwanoha, Kashiwa, Chiba 277-8581, Japan. and*

²*Department of Physics, University of Wisconsin-Milwaukee, Milwaukee, Wisconsin 53211, USA.*

(Dated: September 5, 2018)

A nodeless d -wave state is likely in superconducting monolayer FeSe on SrTiO₃. The lack of nodes is surprising, but has been shown to be a natural consequence of the observed small interband spin-orbit coupling. Here we examine the evolution from a nodeless state to the nodal state as this spin-orbit coupling is increased from a topological perspective. We show that this evolution depends strongly on the orbital content of the superconducting degrees of freedom. In particular, there are two d -wave solutions, which we call orbitally trivial and orbitally non-trivial. In both cases, the nodes carry a ± 2 topological winding number that originates from a chiral symmetry. However, the momentum space distribution of the \pm charges is different for the two cases, resulting in a different evolution of these nodes as they annihilate to form a nodeless superconductor. We further show that the orbitally trivial and orbitally non-trivial nodal states exhibit different Andreev flat band spectra at the edge.

I. INTRODUCTION

Monolayer FeSe grown on SrTiO₃ has generated much attention due to its high superconducting transition temperature T_c , which is higher than all the other Fe-based superconductors. Angle-resolved photoemission spectroscopy (ARPES) [1–3] and scanning tunneling microscopy [4–6] measurements have shown that the superconducting gap, while anisotropic, is fully gapped. Monolayer FeSe lacks the hole pockets about the Γ -point of the Brillouin Zone (BZ) which exist in other iron pnictide compounds. This suggests that the usual s_{\pm} -wave pairing [7, 8] due to spin fluctuations about a collinear antiferromagnetic state with a wave-vector that originates from the momentum difference between electron and hole pockets is unlikely and another mechanism is needed.

Inelastic neutron scattering in single crystal FeSe [9] have found that, in addition to collinear antiferromagnetic fluctuations, there are also fluctuations associated with translation invariant checkerboard antiferromagnetic (CB-AFM) order. First-principles spin-spiral calculations [10] also report enhanced the CB-AFM fluctuations in monolayer FeSe, finding that this system sits at a quantum spin-fluctuation mediated spin paramagnetic ground state. Motivated by the presence of CB-AFM fluctuations, a symmetry based $\mathbf{k} \cdot \mathbf{p}$ theory assuming a single M -point electronic representation was used to describe fermions coupled to these fluctuations [11, 12]. This theory predicts a fully gapped, nodeless d -wave state [12] that naturally gives rise to a gap anisotropy that agrees with experiment. Though typically symmetry arguments imply that such a d -wave state should be nodal [13], this theory reveals that nodal points emerge only if the relevant interband spin-orbit coupling energy is larger than the superconducting gap.

A natural question is what is the mechanism that leads to a nodeless, fully gapped d -wave superconducting state? Indeed, one can ask how such nodeless states are more generally achieved when symmetry arguments would dictate nodes? Here we address this question through an examination of the nodal d -wave state. This question falls naturally into the growing research on topological systems, which originally started with gapped systems [14] such as quantum Hall systems and topological insulators in which surface states are characterized by “bulk-edge correspondence”. More recently this has been extended to gapless systems such as Weyl and Dirac semimetals [15] and unconventional superconductors [16]. In unconventional superconductors that are nodal, that is, have momenta with zero gap, it is known that the sign change of the pairing potential on the Fermi surface leads to dispersionless Andreev bound states at a surface of the system. These states are characterized through topological arguments [17, 18]. Therefore, studies of nodes in unconventional superconductors are important not only to reveal the pairing mechanism but also to clarify the topological surface states.

Although d -wave superconducting states typically have topologically protected nodes in one-band systems, these nodal points can be annihilated in multi-band superconductors [19, 20]. Indeed, it has been pointed out that the merging nodal points near the Γ -point have winding numbers of opposite sign in Fe-based superconductors [21]. In addition, a nodeless d -wave superconductor has also been discussed in the context of cuprates [22]. These works did not include spin-orbit coupling, which is essential in our theory. Our work highlights the annihilation of nodes solely due to spin-orbit coupling and demonstrates that the nodal charge is protected by a chiral symmetry that is the product of time-reversal and particle-hole symmetries. Furthermore, we find that the nodal annihilation depends upon the orbital structure of the d -wave gap. In particular, we find two types of d -wave pairing: (a) orbitally trivial usual d -wave anisotropy with a $k_x k_y$ mo-

*Electronic address: t.nakayama@issp.u-tokyo.ac.jp

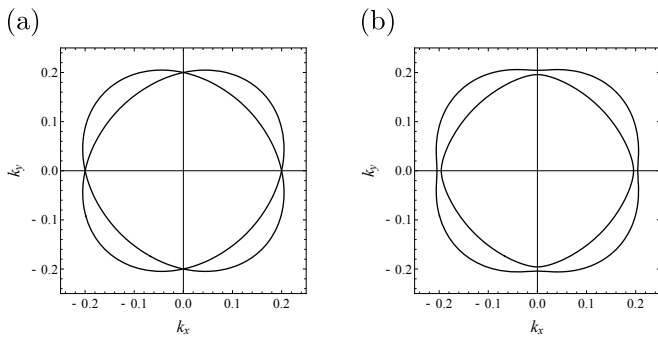


FIG. 1: Fermi surfaces in normal states (a) without spin-orbit coupling and (b) with spin-orbit coupling $v_{so} = 12$ meV. The units of horizontal and vertical axes are \AA^{-1} . The other parameters are given in the main text.

mentum dependence and (b) orbitally non-trivial with no momentum dependence. For the latter case, nodal annihilation arises in a natural and straightforward manner, while for the orbitally trivial case, the annihilation is much less straightforward, proceeding initially through the creation of additional nodes before annihilating as the interband spin-orbit coupling is decreased.

The remainder of this paper is organized as follows. In Sec. II, we introduce the symmetry based effective model that describes the electronic excitations that stem from a single M -point representation of BZ, these representations are four-fold degenerate and thus lead to two bands. We then briefly review the emergence of nodal points due to interband spin-orbit coupling. In Sec. III, we give the topological charges for these nodal points as a $2\mathbb{Z}$ invariant and show that there are topologically distinguished phases which manifest themselves through the presence of dispersionless Andreev surface states. The results are summarized in Sec. IV.

II. MODEL

In this Section, we present a brief review of the low-energy symmetry-based $\mathbf{k} \cdot \mathbf{p}$ -like theory that describes the electronic states of monolayer FeSe in the vicinity of the Fermi level [12]. Density functional theory calculations show that two states, which are \mathbf{k} -dependent linear combinations of Fe $\{xz, yz\}$ and $x^2 - y^2$ orbitals, are dominant at the Fermi level around M -point. These states can be described as originating from a single M -point four-fold electronic representation (with two orbital and two spin degrees of freedom) through an effective $\mathbf{k} \cdot \mathbf{p}$ theory. The simplicity of this model allows insight into the underlying physics that cannot be found using a theoretical model simply based on ten orbital and two spin degrees of freedom. In addition, it captures the relevant physics of the superconducting state that appears in theories of monolayer FeSe that include two M -point representations [23].

In this theory, the normal-state Hamiltonian is

$$H_0(\mathbf{k}) = \epsilon_0 \tau_0 \sigma_0 + \gamma_{xy} \tau_z \sigma_0 + \tau_x [\gamma_x \sigma_y + \gamma_y \sigma_x] \quad (1)$$

where $\mathbf{k} = (k_x, k_y)$ is the momentum measured from M -point of BZ and the τ_i (σ_i) matrices describe the two orbitals (spin) degrees of freedom. The τ_x term is the interband spin-orbit coupling that plays an essential role in the d -wave superconducting state. This term has a magnitude that is related to the on-site spin-orbit coupling, but is also determined by other factors and can be small even if the on-site spin-orbit coupling is substantial. The Fermi surface, as observed by angle-resolved photoemission spectroscopy (ARPES), is reasonably described when we chose $\epsilon_0 = \epsilon_0(\mathbf{k}) = (k_x^2 + k_y^2)/2m - \mu$, $\gamma_{xy} = \gamma_{xy}(\mathbf{k}) = ak_x k_y$, $\gamma_x = \gamma_x(\mathbf{k}) = v_{so} k_x$, $\gamma_y = \gamma_y(\mathbf{k}) = v_{so} k_y$ and parameters as $\mu = 55$ meV, $1/(2m) = 1375$ meV \AA^2 , $a = 600$ meV \AA^2 and $|v_{so}| \leq 15$ meV \AA . Figures 1 show the Fermi surfaces in (a) without spin-orbit coupling and (b) with spin-orbit coupling $v_{so} = 12$ meV \AA .

Superconducting pairing is assumed to be induced by the fluctuations associated with translation invariant CB-AFM. This yields a d_{xy} -like pairing state. Importantly, for this paper, there are two such pairing states that are described in more detail below. The Hamiltonian is given by the following in the Bogoliubov de Gennes form:

$$H(\mathbf{k}) = \Gamma_z (\epsilon_0 \tau_0 \sigma_0 + \gamma_{xy} \tau_z \sigma_0 + \gamma_x \tau_x \sigma_y) + \gamma_y \Gamma_0 \tau_x \sigma_x + i \Gamma_y (\Delta_{d,0} \tau_0 + \Delta_{d,z} \tau_z) i \sigma_y \quad (2)$$

where $\Delta_{d,0} = \Delta_{d,0}(\mathbf{k}) = \Delta_2 k_x k_y / k_0^2$, $\Delta_{d,z} = \Delta_{d,z}(\mathbf{k}) = \Delta_0$, the Γ_i matrices describe the particle-hole degree of freedom, and we take the typical Fermi wave vector $k_0 = 0.2$ \AA^{-1} . The two gap functions $\Delta_{d,0}$ and $\Delta_{d,z}$ are the two d_{xy} pairing degrees of freedom mentioned above. The pairing term $\Delta_{d,0} \tau_0$ represents an orbitally trivial and usual d_{xy} pairing with a $k_x k_y$ momentum dependence. The $\Delta_{d,z} \tau_z$ represents an orbitally non-trivial pairing state with no momentum dependence, it also has d_{xy} pairing symmetry due to the τ_z orbital dependence and the different symmetries of the two orbitals that give rise to this gap function. In general, since both $\Delta_{d,0}$ and $\Delta_{d,z}$ channels have the same symmetry, the gap function will be a linear combination of both these pairing channels.

In order to gain a deeper understanding on these two types of d_{xy} order, it is convenient to change basis from the orbital to the band basis. The Hamiltonian in (2) can be written in block diagonal form with two 4×4 matrices. One of these matrices is

$$\begin{bmatrix} \epsilon_0 + \gamma_{xy} & \gamma_y - i\gamma_x & 0 & \Delta_{d,0} + \Delta_{d,z} \\ \gamma_y + i\gamma_x & \epsilon_0 - \gamma_{xy} & -\Delta_{d,0} + \Delta_{d,z} & 0 \\ 0 & -\Delta_{d,0} + \Delta_{d,z} & -\epsilon_0 + \gamma_{xy} & \gamma_y + i\gamma_x \\ \Delta_{d,0} + \Delta_{d,z} & 0 & \gamma_y - i\gamma_x & -\epsilon_0 - \gamma_{xy} \end{bmatrix}, \quad (3)$$

while the other matrix is given by transforming $\Delta_i \rightarrow -\Delta_i$ and $\gamma_x \rightarrow -\gamma_x$. Performing a unitary transformation that diagonalizes the normal part of the Hamiltonian, we obtain in the band basis, we find

$$\begin{bmatrix} \epsilon_0 + \sqrt{\gamma_x^2 + \gamma_y^2 + \gamma_{xy}^2} & \Delta_{d,0} + \frac{\Delta_{d,z}\gamma_{xy}}{\sqrt{\gamma_x^2 + \gamma_y^2 + \gamma_{xy}^2}} & 0 & \frac{\Delta_{d,z}(\gamma_y - i\gamma_x)}{\sqrt{\gamma_x^2 + \gamma_y^2 + \gamma_{xy}^2}} \\ \Delta_{d,0} + \frac{\Delta_{d,z}\gamma_{xy}}{\sqrt{\gamma_x^2 + \gamma_y^2 + \gamma_{xy}^2}} & -\epsilon_0 - \sqrt{\gamma_x^2 + \gamma_y^2 + \gamma_{xy}^2} & \frac{\Delta_{d,z}(\gamma_y + i\gamma_x)}{\sqrt{\gamma_x^2 + \gamma_y^2 + \gamma_{xy}^2}} & 0 \\ 0 & \frac{\Delta_{d,z}(\gamma_y - i\gamma_x)}{\sqrt{\gamma_x^2 + \gamma_y^2 + \gamma_{xy}^2}} & \epsilon_0 - \sqrt{\gamma_x^2 + \gamma_y^2 + \gamma_{xy}^2} & \Delta_{d,0} - \frac{\Delta_{d,z}\gamma_{xy}}{\sqrt{\gamma_x^2 + \gamma_y^2 + \gamma_{xy}^2}} \\ \frac{\Delta_{d,z}(\gamma_y + i\gamma_x)}{\sqrt{\gamma_x^2 + \gamma_y^2 + \gamma_{xy}^2}} & 0 & \Delta_{d,0} - \frac{\Delta_{d,z}\gamma_{xy}}{\sqrt{\gamma_x^2 + \gamma_y^2 + \gamma_{xy}^2}} & -\epsilon_0 + \sqrt{\gamma_x^2 + \gamma_y^2 + \gamma_{xy}^2} \end{bmatrix} \quad (4)$$

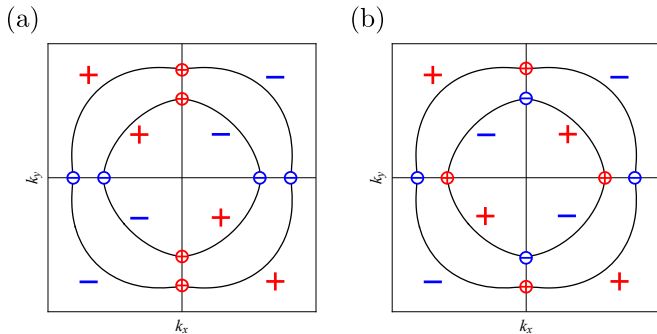


FIG. 2: Pairing anisotropy and topological charges in (a) orbitally trivial pairing and (b) orbitally non-trivial pairing in band basis. The solid lines represent Fermi surface in normal states. The circles represent ± 2 topological charge.

This band basis clarifies that the Hamiltonian has both

intraband and interband pairing. The interband pairing arises only from the orbitally non-trivial $\Delta_{d,z}$ (in combination with the interband spin-orbit coupling). The intraband pairing contains both pairing channels. In this case, the orbitally non-trivial $\Delta_{d,z}$ channel explicitly gains d -wave momentum anisotropy through the γ_{xy} normal state term. Figure 2 shows the pairing anisotropy in case of only (a) orbitally trivial pairing and (b) orbitally non-trivial one in band basis. Note that here only spin-singlet pairing is considered. In general, there can be mixing of spin-singlet and -triplet pairings due to the interband spin-orbit coupling.

The interband pairing in the band basis is essential to generate a gapless superconducting d_{xy} state, provided the interband spin-orbit coupling is sufficiently small. To understand how a large interband spin-orbit coupling gives rise to nodal points, it is useful to consider the quasiparticle dispersion for Hamiltonian (2). This is given by

$$E_{\pm}(\mathbf{k}) = \sqrt{\epsilon_0^2 + \gamma_{xy}^2 + \gamma_x^2 + \gamma_y^2 + \Delta_{d,0}^2 + \Delta_{d,z}^2 \pm 2\sqrt{(\epsilon_0\gamma_{xy} + \Delta_{d,0}\Delta_{d,z})^2 + (\gamma_x^2 + \gamma_y^2)(\epsilon_0^2 + \Delta_{d,z}^2)}}. \quad (5)$$

Along the nodal direction $k_y = 0$, so that $\gamma_{xy} = \gamma_y = \Delta_{d,0} = 0$, yielding $E_{\pm}(\mathbf{k}) = \left| \sqrt{\epsilon_0^2 + \Delta_{d,z}^2} \pm |\gamma_x| \right|$. Therefore, the following equation must be satisfied at the nodal points (labeled \mathbf{k}^*),

$$\epsilon_0^2 = \gamma_x^2 - \Delta_{d,z}^2. \quad (6)$$

This means that once the interband spin-orbit coupling satisfies $|\gamma_x| > \Delta_{d,z}$, nodal points exist. As the interband spin-orbit coupling is reduced, there is consequently a transition from a nodal d_{xy} state to a fully gapped d_{xy} state, which is the focus of the remainder of this paper. Note that a generic consequence of this theory is that gap minima in the fully gapped state are along the nodal directions, this agrees with what is observed in ARPES measurements.

III. NODAL TOPOLOGICAL CHARGES AND ANDREEV FLAT BAND STATES

A. Nodal Topological Charges

Now we examine how the fully gapped d_{xy} state appears as the interband spin-orbit coupling is reduced. In particular, for sufficiently large interband spin-orbit coupling we have a nodal d_{xy} state and we examine the topological charge of the nodal points. We show that topological charge at the nodal points can be defined as a $2\mathbb{Z}$ invariant. The key symmetries in defining this charge are time-reversal (with operator T) and particle-hole conjugation (with operator C). These act on $H(\mathbf{k})$ as

$$TH(\mathbf{k})T^{-1} = H(-\mathbf{k}), \quad (7)$$

$$CH(\mathbf{k})C^{-1} = -H(-\mathbf{k}), \quad (8)$$

where $T = K\Gamma_0\tau_0(i\sigma_y)$, $C = K\Gamma_x\tau_0\sigma_0$, and K is complex conjugate operator. Since $T^2 = -1$ and $C^2 = 1$, this Hamiltonian belongs to Altland-Zirnbauer (AZ) class DIII [24]. Furthermore, we define a chiral operator S ,

$$S = -iTC = \Gamma_x\tau_0\sigma_y. \quad (9)$$

Since S anticommutes with $H(\mathbf{k})$, $H(\mathbf{k})$ can be written in block off-diagonal form using the basis which S is diagonal:

$$H(\mathbf{k}) \rightarrow VH(\mathbf{k})V^\dagger = \begin{bmatrix} 0 & q(\mathbf{k}) \\ q^\dagger(\mathbf{k}) & 0 \end{bmatrix} \quad (10)$$

where

$$q(\mathbf{k}) = \epsilon_0\tau_0\sigma_0 + \gamma_{xy}\tau_z\sigma_0 + \gamma_x\tau_x\sigma_y + \gamma_y\tau_x\sigma_x + i(\Delta_{d,0}\tau_0 + \Delta_{d,z}\tau_z)\sigma_0, \quad (11)$$

Note that $\det q(\mathbf{k}^*) = 0$ because of the nodal condition $E_-(\mathbf{k}^*) = 0$.

In class DIII, a topological charge can be defined by the winding number [25], which is given by

$$W_{\mathcal{L}} = \frac{1}{2\pi i} \oint_{\mathcal{L}} dk_l \text{Tr} [q^{-1}(\mathbf{k})\partial_{k_l}q(\mathbf{k})] \quad (12)$$

where the contour \mathcal{L} is a loop around nodal point. This charge is an integer \mathbb{Z} invariant. In the problem we are considering, we also have parity symmetry which ensures a two-fold degeneracy of the nodal point. Consequently, the nodes have a $2\mathbb{Z}$ topological charge [26]. We find that the orbitally trivial and orbitally non-trivial gap functions exhibit different nodal charge distributions in momentum space and that a topological transition exists between these two cases.

To understand the different nodal charge distributions between the orbitally trivial and non-trivial cases (see Fig. 2), it is useful to consider the limit in which the interband pairing can be ignored. This can be achieved in the orbitally trivial case by setting $\Delta_{d,z} = 0$ and in the orbitally non-trivial case by setting $\Delta_{d,0} = 0$ and also requiring that the interband spin-orbit coupling satisfy $|\gamma_i| \ll |\gamma_{xy}|$. When the interband pairing can be ignored, we can consider the nodal points in each band independently. In this case, following Ref.s [17, 18], Eq. (12) can be simplified to

$$W_{\mathcal{L}^\pm} = - \sum_{\mathbf{k}_0 \in S_{\mathcal{L}^\pm}} \text{sgn} \left(\partial_{k_l} \xi_{\mathbf{k}}^\pm \Big|_{\mathbf{k}=\mathbf{k}_0} \right) \text{sgn} (\Delta_{\mathbf{k}_0}^\pm). \quad (13)$$

where $\xi^\pm = \epsilon_0 \pm \sqrt{\gamma_x^2 + \gamma_y^2 + \gamma_{xy}^2}$, $\Delta_{\mathbf{k}}^\pm$ is the superconducting gap of \pm -helicity and the sum is over the set of points $S_{\mathcal{L}^\pm}$ given by the intersection of \pm -helicity Fermi surface with the one-dimensional contour \mathcal{L}^\pm . We consider explicitly the topological charges of the adjacent pair of nodal points in $k_x (> 0)$ direction, $(k_x^-, 0)$ and $(k_x^+, 0)$. In the orbitally trivial case, the superconducting gap $\Delta_{\mathbf{k}}^\pm$ of each band is $\Delta_{\mathbf{k}}^\pm = -\Delta_{d,0}$, respectively. Therefore, two nodal points will have the same

sign topological charge, which we call *same sign pair* states. On the other hand, for the orbitally non-trivial case, $\Delta_{\mathbf{k}}^\pm \sim \mp \gamma_{xy}\Delta_{d,z}$, so that the two nodal points have opposite sign topological charges, which we call *opposite sign pair* states. In general, the pairing state will be a linear combination of the orbitally trivial and orbitally non-trivial gap functions, but it is intuitively clear that the nodes can still be classified as *same sign pair* or *opposite sign pair* states and a transition between these two topological states can occur. Furthermore, in both cases, as the spin-orbit coupling is decreased, a gapless d_{xy} superconducting state must arise (assuming that $\Delta_{d,z} \neq 0$). The development of this gapless state for *opposite sign pair* states is intuitively clear, but this is not the case for *same sign pair* states.

To gain a deeper understanding into the physics discussed above, we consider a more general treatment of the topological charge. In particular, the topological charge Eq. (12) can be cast in the following form:

$$W_{\mathcal{L}} = \frac{1}{\pi} \oint_{\mathcal{L}} dk_l \partial_{\mathbf{k}} \tan^{-1} \left[\frac{2(\epsilon_0\Delta_{d,0} - \gamma_{xy}\Delta_{d,z})}{\epsilon_0^2 - \gamma_x^2 - \gamma_y^2 - \gamma_{xy}^2 - \Delta_{d,0}^2 + \Delta_{d,z}^2} \right] \quad (14)$$

This can be understood as the winding number of the vector $(\epsilon_0^2 - \gamma_x^2 - \gamma_y^2 - \gamma_{xy}^2 - \Delta_{d,0}^2 + \Delta_{d,z}^2, \epsilon_0\Delta_{d,0} - \gamma_{xy}\Delta_{d,z})$ rotating around the nodal point. The crucial term which determines whether same or opposite sign pairs appear is the numerator $\epsilon_0\Delta_{d,0} - \gamma_{xy}\Delta_{d,z}$ (the denominator $\epsilon_0^2 - \gamma_x^2 - \gamma_y^2 - \gamma_{xy}^2 - \Delta_{d,0}^2 + \Delta_{d,z}^2$ behaves similarly for both same and opposite sign pairs). Substituting detailed forms, the numerator is given by

$$\epsilon_0\Delta_{d,0} - \gamma_{xy}\Delta_{d,z} = \begin{cases} -ak_xk_y\Delta_0 & (\Delta_2 = 0) \\ \frac{k_xk_y}{k_0^2}\Delta_2 \left[\epsilon_0 - ak_0^2\frac{\Delta_0}{\Delta_2} \right] & (\Delta_2 \neq 0) \end{cases} \quad (15)$$

If $\Delta_2 = 0$, the sign of the numerator is the same between the two nodal points \mathbf{k}^{*-} and \mathbf{k}^{*+} , leading to topological charges of opposite sign at the two nodal points, that is *opposite sign pair* states. However, if $\Delta_2 \neq 0$ and sign of $\epsilon_0 - ak_0^2\Delta_0/\Delta_2$ changes between the two nodal point \mathbf{k}^{*-} and \mathbf{k}^{*+} , the topological charges are the same sign at the two nodal points, leading to *same sign pair* states. In order to develop an analytic condition to distinguish these two cases, we consider $k_y = 0$ direction and set \tilde{k}_x as $\epsilon_0(\tilde{k}_x) - ak_0^2\Delta_0/\Delta_2 = 0$. In case of *same sign pair* states, $k_x^* - < k_x < k_x^*$, this is not satisfied for *opposite sign pair* states. With the nodal condition Eq. (6), we get the following inequality,

$$2mv_{\text{so}}^2 - m\sqrt{2\frac{\mu}{m}v_{\text{so}}^2 - \frac{\Delta_0^2}{m^2} + v_{\text{so}}^4} < a\frac{\Delta_0}{\Delta_2}k_0^2 < 2mv_{\text{so}}^2 + m\sqrt{2\frac{\mu}{m}v_{\text{so}}^2 - \frac{\Delta_0^2}{m^2} + v_{\text{so}}^4}. \quad (16)$$

As an example, if we take the values $\Delta_0 = 11$ meV and $\Delta_2 = -1.5$ meV, which was used earlier to generate a

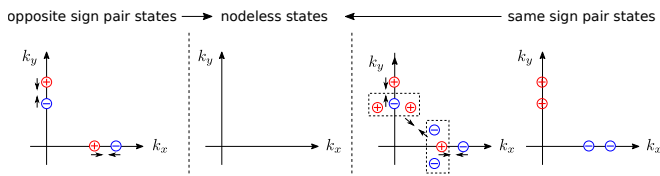


FIG. 3: (Color online) Schematic picture of transition to nodeless states from *opposite* (left) and *same sign pair* states (right). The arrows represent that two nodal points merge with each other. In *same sign pair* states, each inner nodal point splits into three nodal points (surrounded by a dotted line) in transition to nodeless states.

gap anisotropy consistent with experiment, and assume a strong interband spin-orbit coupling $v_{\text{so}} = 80 \text{ meV \AA}$, then the topological character of nodal points is classified as *opposite sign pair* states.

Now we turn to the development of the gapless d_{xy} state due to the merging and annihilation of nodal points. It is worth emphasizing that this has been studied in Dirac and Weyl semimetals [15] and also in s - and d -wave superconductors [21] in a framework different to ours in which spin-orbit coupling is not an essential interaction. In the case of *opposite sign pair* states, the nodal points can merge and annihilate as the interband spin-orbit coupling decreases because they have opposite topological charge. However, in case of *same sign pair* states, merging and annihilation of nodal points cannot occur directly. We find that this occurs through an involved mechanism. Indeed, as the interband spin-orbit coupling is decreased from the *same sign pair* state (which we take to be both positive in the description that follows), a new pair of opposite charge nodal points are created near the nodal point at \mathbf{k}^{*-} . As the interband spin-orbit coupling is further decreased, the negatively charged nodal point stays near \mathbf{k}^{*-} , while the two positively charged nodal points move off the k_x (or k_y) axis. The positively charged nodal points that move off the k_x axis eventually merge with similarly formed negatively charged nodal points that have moved off the k_y axis. This leaves an *opposite sign pair* state, for which the nodes merge and annihilate as before when the interband spin-orbit coupling is further decreased. (See Fig. 3).

B. Andreev flat band states

We find that typically either *same sign pair* states or *opposite sign pair* states occur when the superconducting state is nodal. In particular, the state we find above with 16 nodal points only exists in a narrow range of parameters, so we do not consider it further here. It would be of interest to be able to experimentally identify whether *same sign* or *opposite sign pair* states exist. This can be done through an examination of edge states. The non-trivial topological charges at nodal points im-

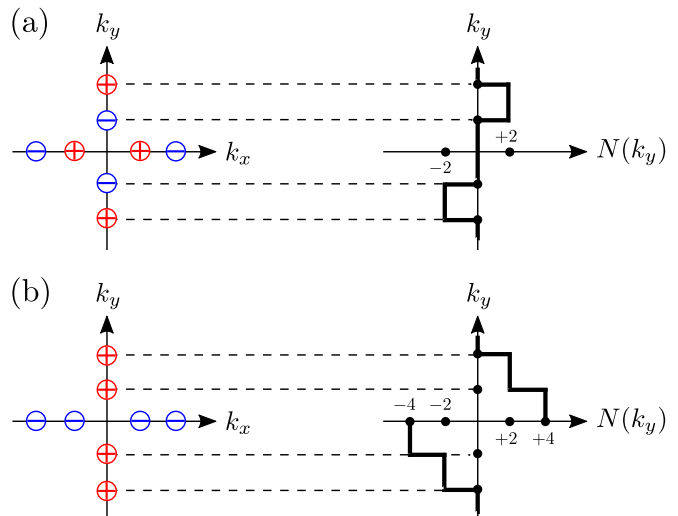


FIG. 4: (Color online) Schematic pictures of the relation between $W_{\mathcal{L}}$ (left) and $N(k_y)$ (right) in case of (a) *opposite sign pair* and (b) *same sign pair* states. Red and blue points indicate $W_{\mathcal{L}} = +2$ and -2 , respectively.

ply the existence of dispersionless Andreev band states or Andreev flat band states as edge states. The number of Andreev flat band states is related to a 1D winding number $N(\mathbf{k}_{\parallel})$ [18, 27] which is given by

$$N(\mathbf{k}_{\parallel}) = \int d\mathbf{k}_{\perp} \text{Tr} [q^{-1}(\mathbf{k}) \partial_{\mathbf{k}_{\perp}} q(\mathbf{k})], \quad (17)$$

where \mathbf{k}_{\parallel} (\mathbf{k}_{\perp}) is bulk momentum parallel (perpendicular) to the surface. We consider edges running along the y direction and take \mathbf{k}_{\parallel} (\mathbf{k}_{\perp}) as k_y (k_x). Figure 4 shows that the relation between the 1D winding number $N(k_y)$ and the topological charge $W_{\mathcal{L}}$. Figure 4 (a) shows the 1D winding number is nonzero between nodal points which have opposite sign topological charge but is zero at the origin in case of *opposite sign pair* states. On the other hand, the 1D winding number is nonzero for all momenta between the outer nodal points in case of *same sign pair* states (Figure 4 (b)).

In order to investigate the edge states further, we introduce a lattice model which corresponds to Eq. (2) (See appendix A). We suppose that the system has two edges at $i_x = 1$ and N_x in x direction and take the boundary condition in the y direction to be periodic. Then, we examine the edge states by numerically obtaining the energy spectrum as a function of the momentum k_y . We set $N_x = 10000$. Figure 5 shows the energy spectra for (a) no nodal points, (b), (c) *opposite sign pair* states and (d) *same sign pair* states. Indeed, with no nodal points we do not have Andreev flat band states and once the nodal points appear with increasing interband spin-orbit coupling, flat band states appear. In cases of (b) and (c) *opposite sign pair* states, the flat band states exist between two nodal points that have opposite topological charge and the number of the flat band states is two

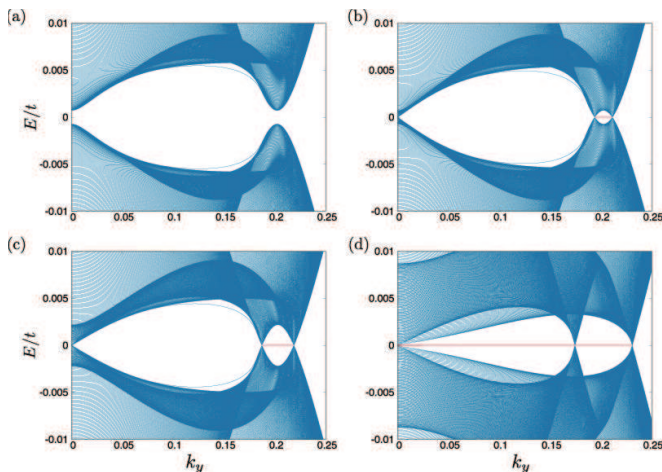


FIG. 5: Energy spectra for (a) no nodal points (b) opposite sign pair (c) opposite sign pair (d) same sign pair states. We set the parameters as $(v_{\text{so}}[\text{meV}\text{\AA}], \Delta_0[\text{meV}], \Delta_2[\text{meV}]) =$ (a) $(50, 11, -1.5)$, (b) $(60, 11, -1.5)$, (c) $(70, 11, -1.5)$ and (d) $(80, 4, -10)$. The vertical axis is scaled by $t = (2m)^{-1}$.

for each edge. On the other hand, in cases of (d) *same sign pair* states, the flat band states exist at $k_y = 0$ and the number of the flat band states across $k_y = 0$ and between two nodal points in positive k_y is four and two for each edge, respectively. In these cases, the number of flat band states has a one to one correspondence with $|N(k_y)|$ which is shown in Fig. 4. Note that in Fig. 4 (d) finite size effect creates a gap at $k_y = 0$. We have confirmed that there is no gap at $k_y = 0$ by using the recursive Green's function method (see Appendix B). In addition to the flat band edge states that appear when nodes exist in the bulk spectrum, note that we find edge states within the gap, though not at zero energy, even in the fully gapped case. These can be attributed to sign changes in the gap that still appear in a fully gapped d_{xy} superconductor.

IV. CONCLUSION

We have studied nodal topological charges in d -wave superconducting monolayer FeSe to help understand the origin of a fully gapped d -wave state. The nodal points that arise when interband spin-orbit coupling is sufficiently strong have $2\mathbb{Z}$ topological charges that give rise to zero-energy dispersionless Andreev edge bound states. The momentum space distribution of the nodal charges depends strongly on the orbital character of the superconducting state, allowing this to be probed through the observation of Andreev bound states.

Acknowledgments

We thank Philip Brydon, Andrey Chubukov, Hirokazu Tsunetsugu, and Mike Weinert for useful discussions. Our numerical calculations were partly carried out at the Supercomputer Center, The Institute for Solid State Physics, The University of Tokyo. T. N was supported by JSPS through Program for Leading Graduate Schools (MERIT).

Appendix A: lattice model

In order to obtain the lattice model which corresponds to Eq. (2), we replace $k_i \rightarrow \sin k_i$ and $-(k_x^2 + k_y^2)/(2m) \rightarrow -2t(\cos k_x + \cos k_y) + 4t$ where $t^{-1} = 2m$ in Eq. (2) (lattice constant is unit). We use $A_{i\sigma}$ and $B_{i\sigma}$ which are annihilation operators of two orbital, spin $\sigma = \uparrow$ and \downarrow electron at i , we divide \mathcal{H} into \mathcal{H}_0 , \mathcal{H}_{SOC} and \mathcal{H}_Δ . These are given by

$$\begin{aligned} \mathcal{H}_0 = & -t \sum_{\langle i,j \rangle, \sigma} \left[A_{i\sigma}^\dagger A_{j\sigma} + B_{i\sigma}^\dagger B_{j\sigma} \right] - (\mu - 4t) \sum_{i, \sigma} \left[A_{i\sigma}^\dagger A_{i\sigma} + B_{i\sigma}^\dagger B_{i\sigma} \right] \\ & + \frac{a}{4} \sum_{i, \sigma} \left[A_{i\sigma}^\dagger A_{i+x+y\sigma} + A_{i+x+y\sigma}^\dagger A_{i\sigma} - \left(A_{i\sigma}^\dagger A_{i+x-y\sigma} + A_{i+x-y\sigma}^\dagger A_{i\sigma} \right) \right] \\ & - \frac{a}{4} \sum_{i, \sigma} \left[B_{i\sigma}^\dagger B_{i+x+y\sigma} + B_{i+x+y\sigma}^\dagger B_{i\sigma} - \left(B_{i\sigma}^\dagger B_{i+x-y\sigma} + B_{i+x-y\sigma}^\dagger B_{i\sigma} \right) \right], \end{aligned} \quad (\text{A1})$$

$$\begin{aligned} \mathcal{H}_{\text{SOC}} = & -\frac{v_{\text{so}}}{2} \sum_i \left[\left\{ A_{i\uparrow}^\dagger B_{i+x\downarrow} - A_{i+x\uparrow}^\dagger B_{i\downarrow} \right\} - \left\{ A_{i\downarrow}^\dagger B_{i+x\uparrow} - A_{i+x\downarrow}^\dagger B_{i\uparrow} \right\} \right] \\ & \left\{ B_{i\uparrow}^\dagger A_{i+x\downarrow} - B_{i+x\uparrow}^\dagger A_{i\downarrow} \right\} - \left\{ B_{i\downarrow}^\dagger A_{i+x\uparrow} - B_{i+x\downarrow}^\dagger A_{i\uparrow} \right\} \\ & + \frac{v_{\text{so}}}{2i} \sum_i \left[\left\{ A_{i\uparrow}^\dagger B_{i+y\downarrow} - A_{i+y\uparrow}^\dagger B_{i\downarrow} \right\} + \left\{ A_{i\downarrow}^\dagger B_{i+y\uparrow} - A_{i+y\downarrow}^\dagger B_{i\uparrow} \right\} \right] \\ & \left\{ B_{i\uparrow}^\dagger A_{i+y\downarrow} - B_{i+y\uparrow}^\dagger A_{i\downarrow} \right\} + \left\{ B_{i\downarrow}^\dagger A_{i+y\uparrow} - B_{i+y\downarrow}^\dagger A_{i\uparrow} \right\} \end{aligned} \quad (\text{A2})$$

$$\begin{aligned} \mathcal{H}_\Delta = & -\frac{\Delta_2}{4k_0^2} \sum_i \left[A_{i\uparrow}^\dagger A_{i-x-y\downarrow}^\dagger + A_{i\uparrow}^\dagger A_{i+x+y\downarrow}^\dagger - \left(A_{i\uparrow}^\dagger A_{i-x+y\downarrow}^\dagger + A_{i\uparrow}^\dagger A_{i+x-y\downarrow}^\dagger \right) \right] \\ & - \left\{ A_{i\downarrow}^\dagger A_{i-x-y\uparrow}^\dagger + A_{i\downarrow}^\dagger A_{i+x+y\uparrow}^\dagger - \left(A_{i\downarrow}^\dagger A_{i-x+y\uparrow}^\dagger + A_{i\downarrow}^\dagger A_{i+x-y\uparrow}^\dagger \right) \right\} \\ & - \frac{\Delta_2}{4k_0^2} \sum_i \left[B_{i\uparrow}^\dagger B_{i-x-y\downarrow}^\dagger + B_{i\uparrow}^\dagger B_{i+x+y\downarrow}^\dagger - \left(B_{i\uparrow}^\dagger B_{i-x+y\downarrow}^\dagger + B_{i\uparrow}^\dagger B_{i+x-y\downarrow}^\dagger \right) \right] \\ & - \left\{ B_{i\downarrow}^\dagger B_{i-x-y\uparrow}^\dagger + B_{i\downarrow}^\dagger B_{i+x+y\uparrow}^\dagger - \left(B_{i\downarrow}^\dagger B_{i-x+y\uparrow}^\dagger + B_{i\downarrow}^\dagger B_{i+x-y\uparrow}^\dagger \right) \right\} \\ & + \Delta_0 \sum_i \left[A_{i\uparrow}^\dagger A_{i\downarrow}^\dagger - A_{i\downarrow}^\dagger A_{i\uparrow}^\dagger - \left(B_{i\uparrow}^\dagger B_{i\downarrow}^\dagger - B_{i\downarrow}^\dagger B_{i\uparrow}^\dagger \right) \right] \\ & + \text{h.c.} \end{aligned} \quad (\text{A3})$$

Appendix B: Energy spectrum by Green's function method

Our Hamiltonian matrix of the edge problem has a simple band form

$$\mathcal{H} = \begin{pmatrix} A & B & 0 & 0 & 0 & 0 & \cdots \\ B^\dagger & A & B & 0 & 0 & 0 & \cdots \\ 0 & B^\dagger & A & B & 0 & 0 & \cdots \\ 0 & 0 & B^\dagger & A & B & 0 & \cdots \\ \vdots & \vdots & \vdots & \vdots & \vdots & \vdots & \ddots \end{pmatrix}, \quad (\text{B1})$$

where A and B are small square matrices of order 8 (or 4 in the reduced block form). López Sancho *et al.*[28] have developed a highly convergent iterative scheme to calculate the surface and bulk Green's functions (G_{00} and $G_{\infty\infty}$ respectively) for this form of Hamiltonian. At i -th iteration, the (renormalized) G_{00} is given in terms of effective interaction with 2^i -th layer:

$$(\omega I - \epsilon_i^S) G_{00} = I + \alpha_i G_{2^i, 0} \quad (\text{B2})$$

and other elements given by

$$(\omega I - \epsilon_i) G_{2^i n, 0} = \beta_i G_{2^i(n-1), 0} + \alpha_i G_{2^i(n+1), 0}, \quad (\text{B3})$$

$$(\omega I - \epsilon_i) G_{2^i n, 2^i n} = I + \beta_i G_{2^i(n-1), 2^i n} + \alpha_i G_{2^i(n+1), 2^i n} \quad (\text{B4})$$

where ω is an energy with small imaginary part $i\eta$ and (ω -dependent) energy matrices ϵ_i^s , ϵ_i , α_i , and β_i are determined recursively starting from $\epsilon_0^s = \epsilon_0 = A$, $\alpha_0 = B$, and $\beta_0 = B^\dagger$. As the iteration proceeds, the effective interactions α_i and β_i decay quickly. We take $\eta/t = 10^{-5}$ and the iteration is truncated when $|\alpha_i/t|, |\beta_i/t| < 10^{-7}$. Required number of iterations are at most 20.

Figure 6 shows k_y -resolved spectral functions obtained by this method,

$$N_n(k_y, E) = -\frac{1}{\pi} \text{Im Tr } G_{nn}(k_y, E + i\eta) \quad (\text{B5})$$

with $n = 0$ (edge) and $n = \infty$ (bulk), for the four parameter sets used in the main-text Fig. 5 (a)-(d). Blowup of spectral functions near $k_y \sim 0$ are shown in Fig. 7.

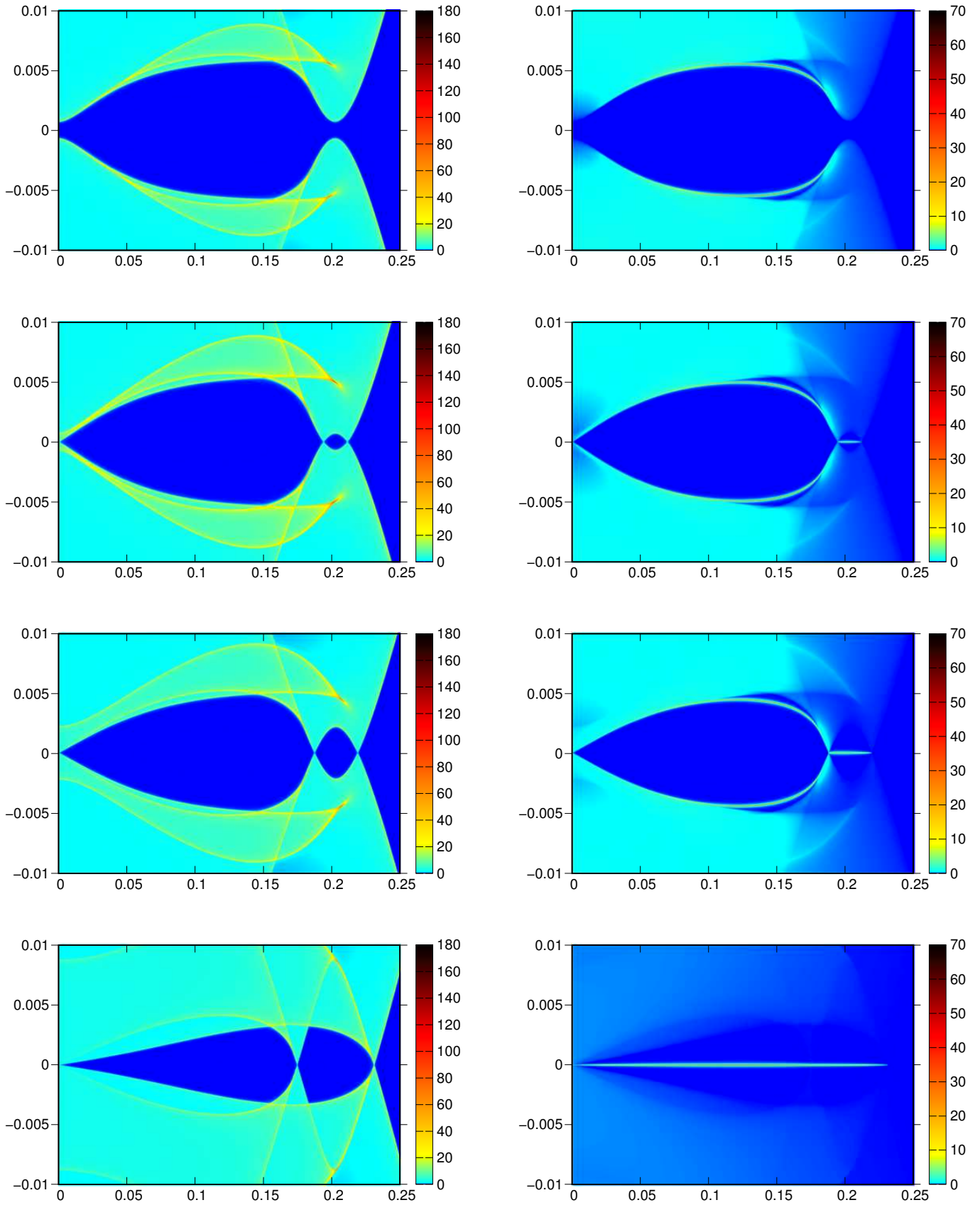


FIG. 6: (Color online) Momentum-resolved spectral function calculated by Green's function method. Left (Right) panels provide local density of states at bulk (edge). Dark blue area represents no-state region. (a) full gap, (b)(c) opposite sign pair of nodal points, (d) same sign pair of nodal points. The energy is given in unit of t .

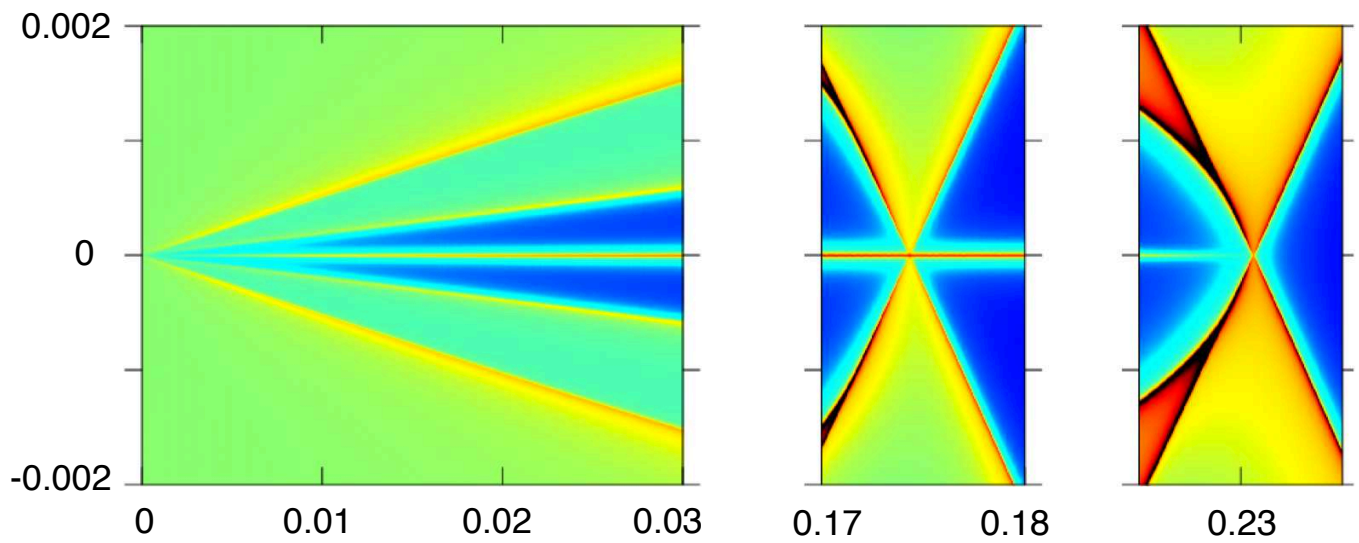


FIG. 7: (Color online) Blowup of spectral function (edge+bulk) of the parameter set (d) around gapless regions with fine resolution in energy and momentum.

-
- [1] Defa Liu, Wenhao Zhang, Daixiang Mou, Junfeng He, Yun-Bo Ou, Qing-Yan Wang, Zhi Li, Lili Wang, Lin Zhao, Shaolong He, Yingying Peng, Xu Liu, Chaoyu Chen, Li Yu, Guodong Liu, Xiaoli Dong, Jun Zhang, Chuangtian Chen, Zuyan Xu, Jiangping Hu, Xi Chen, Xucun Ma, Qikun Xue and X.J. Zhou, Electronic origin of high-temperature superconductivity in single-layer FeSe superconductor, *Nat. Commun.* **3**, 931 (2012).
- [2] Shaolong He, Junfeng He, Wenhao Zhang, Lin Zhao, Defa Liu, Xu Liu, Daixiang Mou, Yun-Bo Ou, Qing-Yan Wang, Zhi Li, Lili Wang, Yingying Peng, Yan Liu, Chaoyu Chen, Li Yu, Guodong Liu, Xiaoli Dong, Jun Zhang, Chuangtian Chen, Zuyan Xu, Xi Chen, Xucun Ma, Qikun Xue and X. J. Zhou, Phase diagram and electronic indication of high-temperature superconductivity at 65 K in single-layer FeSe films, *Nat. Mater.* **12**, 605 (2013).
- [3] Shiyong Tan, Yan Zhang, Miao Xia, Zirong Ye, Fei Chen, Xin Xie, Rui Peng, Difei Xu, Qin Fan, Haichao Xu, Juan Jiang, Tong Zhang, Xinchun Lai, Tao Xiang, Jiangping Hu, Binping Xie and Donglai Feng, Interface-induced superconductivity and strain-dependent spin density waves in FeSe/SrTiO₃ thin films, *Nat. Mater.* **12**, 634 (2013).
- [4] Wang Qing-Yan, Li Zhi, Zhang Wen-Hao, Zhang Zuo-Cheng, Zhang Jin-Song, Li Wei, Ding Hao, Ou Yun-Bo, Deng Peng, Chang Kai, Wen Jing, Song Can-Li, He Ke, Jia Jin-Feng, Ji Shuai-Hua, Wang Ya-Yu, Wang Li-Li, Chen Xi, Ma Xu-Cun and Xue Qi-Kun, Interface induced high temperature superconductivity in single unit-cell FeSe films on SrTiO₃, *Chin. Phys. Lett.* **29**, 037402 (2012).
- [5] Zhi Li, Jun-Ping Peng, Hui-Min Zhang, Wen-Hao Zhang, Hao Ding, Peng Deng, Kai Chang, Can-Li Song, Shuai-Hua Ji, Lili Wang, Ke He, Xi Chen, Qi-Kun Xue and Xu-Cun Ma, Molecular beam epitaxy growth and post-growth annealing of FeSe films on SrTiO₃: a scanning tunneling microscopy study, *J. Phys.: Condens. Matter* **26**, 265002 (2014).
- [6] Q. Fan, W. H. Zhang, X. Liu, Y. J. Yan, M. Q. Ren, R. Peng, H. C. Xu, B. P. Xie, J. P. Hu, T. Zhang and D. L. Feng, Plain *s*-wave superconductivity in single-layer FeSe on SrTiO₃ probed by scanning tunnelling microscopy, *Nat. Phys.* **11**, 946 (2015).
- [7] I. I. Mazin, D. J. Singh, M. D. Johannes, and M. H. Du, Unconventional Superconductivity with a Sign Reversal in the Order Parameter of LaFeAsO_{1-x}F_x, *Phys. Rev. Lett.* **101**, 057003 (2008).
- [8] Kazuhiko Kuroki, Seiichiro Onari, Ryotaro Arita, Hidetomo Usui, Yukio Tanaka, Hiroshi Kontani, and Hideo Aoki, Unconventional Pairing Originating from the Disconnected Fermi Surfaces of Superconducting LaFeAsO_{1-x}F_x, *Phys. Rev. Lett.* **101**, 087004 (2008).
- [9] Qisi Wang, Yao Shen, Bingying Pan, Xiaowen Zhang, K. Ikeuchi, K. Iida, A. D. Christianson, H. C. Walker, D. T. Adroja, M. Abdel-Hafiez, Xiaojia Chen, D. A. Chareev, A. N. Vasiliev and Jun Zhao, Magnetic ground state of FeSe, *Nature Commun.* **7**, 12182 (2016).
- [10] T. Shishidou, D. F. Agterberg and M. Weinert, Magnetic fluctuations in single-layer FeSe, *Communications Physics*, **1**, 8 (2018).
- [11] Vladimir Cvetkovic and Oskar Vafek, Space group symmetry, spin-orbit coupling, and the low-energy effective Hamiltonian for iron-based superconductors, *Phys. Rev. B* **88**, 134510 (2013).
- [12] D. F. Agterberg, T. Shishidou, J. O'Halloran, P. M. R. Brydon, and M. Weinert, Resilient Nodeless *d*-Wave Superconductivity in Monolayer FeSe, *Phys. Rev. Lett.* **119**, 267001 (2017).
- [13] Manfred Sigrist and Kazuo Ueda, Phenomenological theory of unconventional superconductivity, *Rev. Mod. Phys.* **63**, 239 (1991).
- [14] M. Z. Hasan and C. L. Kane, Colloquium: Topological insulators, *Rev. Mod. Phys.* **82**, 3045 (2010).
- [15] Oskar Vafek and Ashvin Vishwanath, Dirac Fermions in Solids: From High-*T_c* Cuprates and Graphene to Topological Insulators and Weyl Semimetals, *Annu. Rev. Condens. Matter Phys.* **5**, 83 (2014).
- [16] Andreas P Schnyder and Philip M R Brydon, Topological surface states in nodal superconductors, *J. Phys.: Condens. Matter* **27** 243201 (2015).
- [17] Andreas P. Schnyder, P. M. R. Brydon, and Carsten Timm, Types of topological surface states in nodal noncentrosymmetric superconductors, *Phys. Rev. B* **85**, 024522 (2012).
- [18] Masatoshi Sato, Yukio Tanaka, Keiji Yada, and Takehito Yokoyama, Topology of Andreev bound states with flat dispersion, *Phys. Rev. B* **83**, 224511 (2011).
- [19] Andrey V. Chubukov, Oskar Vafek and Rafael M. Fernandes, Displacement and annihilation of Dirac gap nodes in *d*-wave iron-based superconductors, *Phys. Rev. B* **94**, 174518 (2016).
- [20] Emilian M. Nica, Rong Yu and Qimiao Si, Orbital-selective pairing and superconductivity in iron selenides, *Npj Quantum Mater.* **2**, 24 (2017).
- [21] Dmitry V. Chichinadze and Andrey V Chubukov, Winding numbers of nodal points in Fe-based superconductors, *Phys. Rev. B* **97**, 094501 (2018).
- [22] Guo-Yi Zhu, Fu-Chun Zhang, and Guang-Ming Zhang, Proximity-induced superconductivity in monolayer CuO₂ on cuprate substrates, *Phys. Rev. B* **94**, 174501 (2016).
- [23] P. M. Eugenio and O. Vafek, Classification of symmetry derived pairing at the *M* point in FeSe, *Phys. Rev. B* **98**, 014503 (2018).
- [24] Andreas P. Schnyder, Shinsei Ryu, Akira Furusaki, and Andreas W. W. Ludwig, Classification of topological insulators and superconductors in three spatial dimensions, *Phys. Rev. B* **78**, 195125 (2008).
- [25] B. Béri, Topologically stable gapless phases of time-reversal-invariant superconductors, *Phys. Rev. B* **81**, 134515 (2010).
- [26] Tomáš Bzdušek and Manfred Sigrist, Robust doubly charged nodal lines and nodal surfaces in centrosymmetric systems, *Phys. Rev. B* **96**, 155105 (2017).
- [27] Andreas P. Schnyder and Shinsei Ryu, Topological phases and surface flat bands in superconductors without inversion symmetry, *Phys. Rev. B* **84**, 060504(R) (2011).
- [28] M. P. Lopez Sancho, J. M. Lopez Sancho, and J Rubio, Highly convergent schemes for the calculation of bulk and surface Green functions, *J. Phys. F* **14**, 1205 (1985).